

Revealing the Instantaneous Machining Gap Produced During wire Electrochemical Micromachining Using Electrochemical Deposition

Xiaolei Bi¹, Yongbin Zeng^{1,2 *}

¹ Nanjing University of Aeronautics and Astronautics, Nanjing 210016, China

² Jiangsu Key Laboratory of Precision and Micro-Manufacturing Technology, Nanjing 210016, China

*E-mail: binyz@nuaa.edu.cn

Received: 3 July 2020 / Accepted: 21 August 2020 / Published: 30 September 2020

Wire electrochemical micromachining (WECMM) has increasingly been recognized as a promising method in producing micro-components. Research into the machining gap is of great importance for understanding the regularities of WECMM. However, studies published on the machining gap are usually approximate and simplified because it is difficult to observe and measure the formation and distribution of the instantaneous machining gap. In this paper, electrochemical deposition is proposed as an innovative method for revealing the instantaneous machining gap produced during WECMM. The method is shown to be feasible in principle by a simulation. Optimum values of 1.0 A/dm² for the current density and 3 h for the machining time are determined experimentally. Several techniques for obtaining a clear contour of the machining gap are tested, and focused ion beam milling is finally selected as the best way to remove the redundant wire and metal deposited beyond the workpiece surface in the position of the machining gap. Using the proposed method, the contour of the machining gap during WECMM of pure nickel is clearly revealed for the first time.

Keywords: Wire electrochemical micromachining (WECMM), Machining gap, Electrochemical deposition, Focused ion beam milling (sputtering and etching)

1. INTRODUCTION

With the increasing demand for micro-components in micro-machines and micro-electromechanical systems (MEMS), various advanced microfabrication techniques, such as UV-LIGA, electric discharge micromachining, electrochemical micromachining, and laser micromachining, have been developed [1]. Wire electrochemical micromachining (WECMM), a particular type of electrochemical micromachining (ECMM), has come to be widely recognized as a flexible and effective technique for fabricating micro-components from a wide range of electrically conductive materials [2].

It combines the advantages of electrochemical micromachining and wire cutting, and it can produce precise nanometer-scale localized machining using nanosecond pulses [3].

During WECMM, micrometer or even sub-micrometer scale machining gap is produced between the wire and the workpiece as the localized anodic dissolution. A smaller side-gap often represents higher forming accuracy and ultimate machining ability. However, bubbles and by-products accumulated in the machining gap significantly influence electrolyte conductivity, thereby affect machining efficiency, machining stability, and machining accuracy [4, 5]. The continuous forming and homogeneous distribution for machining gap is closely dependent on the mass transfer efficiency in the machining gap and various machining factors, it is the premise to obtain better machining efficiency, machining stability, and machining accuracy [6]. Therefore, to obtain a sound theoretical understanding of the WECMM, it is necessary to investigate the formation and distribution of the machining gap. The results of such an investigation should enable a good assessment of the machining state, an accurate analysis of the influence of various factors on machining, and the selection of an appropriate mass transfer scheme.

To date, there have been a number of fruitful studies of WECMM. Different metallic materials have different electrochemical characteristics, and so studies of the WECMM process have been carried out for a range of such materials, for example, pure-aluminum [7], stainless steel [8], cobalt-based alloy [9], TiAl alloy [10], and $\text{Ni}_{72}\text{Cr}_{19}\text{Si}_7\text{B}_2$ glassy alloy [11]. Another branch of recent and ongoing research aims to improve the mass transfer efficiency in the micromachining gap, methods about the use of axial electrolyte flushing [12], electrode vibration technique [13], ribbed wire electrode [14], reciprocating traveling workpiece [15], and wire electrode with surface microstructures [16], have been proposed for obtaining better machining results. However, much of this research is experimental, and there have been relatively few theoretical studies of WECMM, especially on the formation and distribution of the machining gap.

According to the published studies, Zhu *et al.* [17] constructed a theoretical model of the WECMM using Faraday's law and the Butler–Volmer equation to evaluate machining accuracy. Volgin *et al.* [18] established a mathematical model of the WECMM based on the Laplace equation, with the aim of optimizing the forming of complex surfaces using anodic machining. However, these models are the simplified and approximate results, far from revealing the regularities of WECMM. In actual machining, the machining area is generally at the micrometer scale or even smaller, and the machining process occurs in solution, and to date no effective means have been reported that are able to conduct real-time observations and measurements of the instantaneous state of the machining gap under the influence of various machining factors. This has obstructed further experimental study of the formation and distribution of the machining gap under actual machining conditions, and has led to a hiatus in theoretical research on WECMM.

In this paper, in an innovative approach, electrochemical deposition is proposed as a method to reveal the instantaneous machining gap produced during WECMM. The underlying principle is shown to be valid by a simulation. The appropriate current density and machining time for electrochemical deposition are selected after an experimental investigation. Several techniques for obtaining a clear machining gap contour are investigated. Using the proposed method, and with WECMM of pure nickel being taken as an example, an instantaneous machining gap is revealed for the first time.

2. PRINCIPLE AND ANALYSIS

Fig. 1 illustrates the principle of revealing the instantaneous machining gap produced during WECMM using electrochemical deposition. Fig. 1(a) shows the process of the WECMM [2], when the WECMM enters a stable state, the feed of the wire electrode and the nanosecond pulses are simultaneously stopped, the instantaneous position of the wire relative to the micro-slit is retained. Fig. 1(b) shows the process of the electrochemical deposition, under the action of the auxiliary anode, reduced metal ions are deposited onto the surface of the wire electrode and gradually fill the machining gap, and the relative position of the wire and micro-slit is fixed by the electrochemical deposition layer.

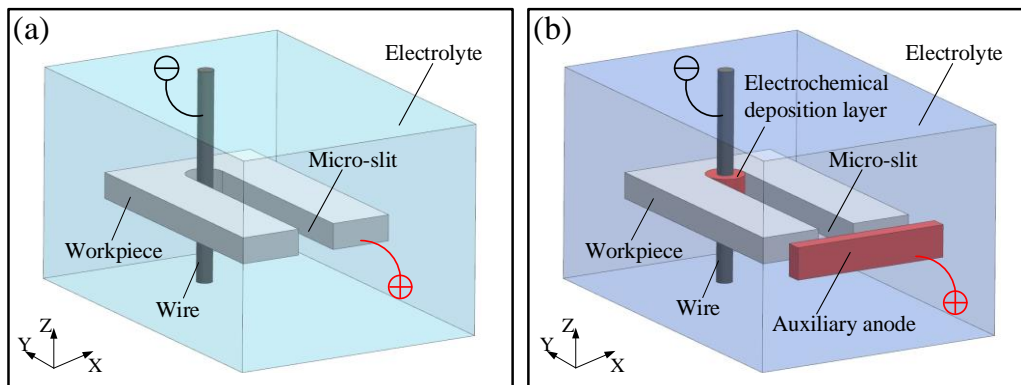


Figure 1. Schematic of the proposed method: (a) the process of WECMM; (b) the process of electrochemical deposition.

After electrochemical dissolution of the workpiece has been completed, the redundant wire and metal deposited beyond the workpiece surface in the machining gap position are removed, and the contour of the machining gap is clearly revealed by the electrochemical deposition layer, as shown in Fig. 2. The state of the machining gap as revealed in this way will provide an accurate representation of the instantaneous machining gap during WECMM shown in Fig. 1(a). Therefore, the accurate observation and measurement for the distribution of the machining gap under different machining factors can be realized, thus providing an experimental possibility for further revealing the regularities of WECMM.

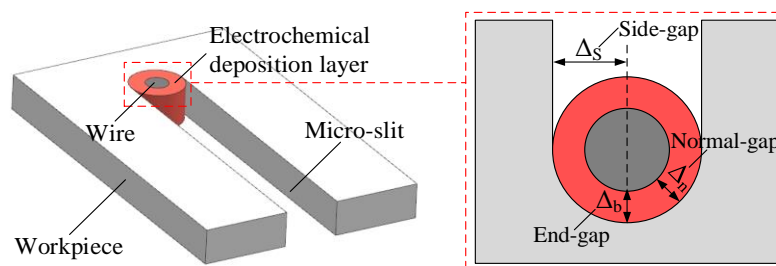


Figure 2. Schematic of the machining gap after electrochemical deposition.

Table 1. Parameter values used in the electric field simulation.

| Parameter | Value |
|-------------------------------------|--------------------------------------|
| Wire diameter | 20 μm |
| Slit width and slit length | 30 μm , 200 μm |
| Electrolyte electrical conductivity | 14.3 S/m |
| Workpiece electrical conductivity | 14,300,000 S/m |
| Applied potential difference | 1 V |

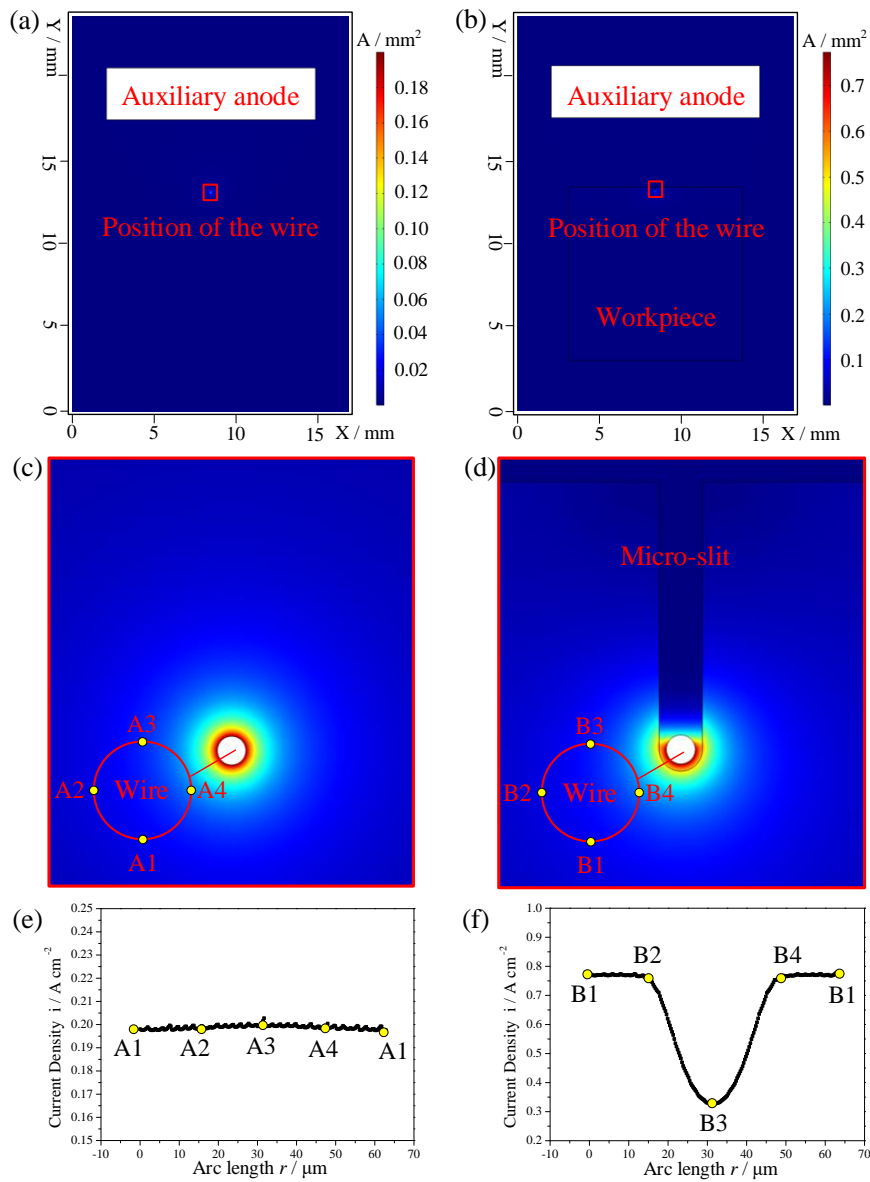


Figure 3. Overall current density distributions in the electrochemical deposition area: (a) when there is deposition on the wire in the absence of the workpiece, and (b) when the workpiece is present and there is deposition on the wire inside the micro-slit. The local current density distribution: (c) on the wire position, and (d) in the machining gap area. Current density values on the wire surface: (e) when there is deposition on the wire in the absence of the workpiece, and (f) when the workpiece is present and there is deposition on the wire inside the micro-slit.

Fig. 3 presents the results of a simulation of the electric field to further illustrate the principle of the proposed method. The simulation was carried out using COMSOL 5.2a. The parameters applied in the simulation are listed in Table 1.

Fig. 3(a) shows the overall current density distribution in the electrochemical deposition area when deposition occurs on the wire in the absence of the workpiece. Fig. 3(c) and Fig. 3(e) show the current density distribution on the wire position and the corresponding current density values on the wire surface, respectively. It can be seen that the wire surface has current distribution, and the current density is relatively uniform. As a result, the reduced metal ions can be deposited on the wire surface. Fig. 3(b) shows the overall current density distribution in the electrochemical deposition area when the workpiece is present and deposition occurs on the wire inside the micro-slit. Fig. 3(d) and Fig. 3(f) show the current density distribution in the machining gap area and the corresponding current density values on the wire surface, respectively. It can be seen that there is again a current distribution on the wire surface and that the values of the current density on the wire surface are all larger than in the absence of the workpiece. In addition, the current density on the wire surface inside the machining gap (arcs B1B2 and B4B1) is larger than that on the wire surface outside the machining gap (arcs B2B3 and B3B4). This indicates that when the wire is inside the micro-slit, electrochemical deposition will occur normally and that reduced metal ions will be deposited more readily at the position of the machining gap. Thus, the proposed method is theoretically feasible.

3. EXPERIMENTAL DETAILS

Fig. 4 shows the experimental system developed for this work. It consists of a PC controller, an XYZ three-axis motion stage, a digital relay, a pulse generator, a DC power supply, an auxiliary anode, an oscilloscope, an electrolyte tank, an electrolyte circulation system, the wire fixture, and the workpiece.

During WECMM, the on-off switching of the pulse generator and the synchronous stopping of the XYZ three-axis motion stage were controlled by the digital relay. The DC power supply and the auxiliary anode were used for the process of electrochemical deposition. The electrolyte for WECMM, the electrolyte for electrochemical deposition, and deionized water were put into tanks 1, 2, and 3, respectively, in the electrolyte circulation system. The deionized water was used to clean the electrolyte tank after each process, and tank 4 was used to collect the spent electrolyte.

In this paper, a 125- μm -thick foil of pure-nickel was used as the workpiece and 20- μm -diameter tungsten wire was used as the wire cathode. After the WECMM, the electrolyte was replaced. The electrochemical deposition electrolyte was a mixture of $\text{CuSO}_4 \cdot 5\text{H}_2\text{O}$ at a concentration of 90 g/L and H_2SO_4 at a concentration of 160 g/L. The auxiliary anode was made of phosphor copper. All the experiments were carried out at room temperature, and the electrolyte was stationary during the electrochemical deposition.

During the experiments, the computer-controlled digital camera (CCD) provided magnified online observations. The overall and local topography of the experimental results were examined using a digital camera, a digital microscope (Leica), and a scanning electron microscope (SEM).

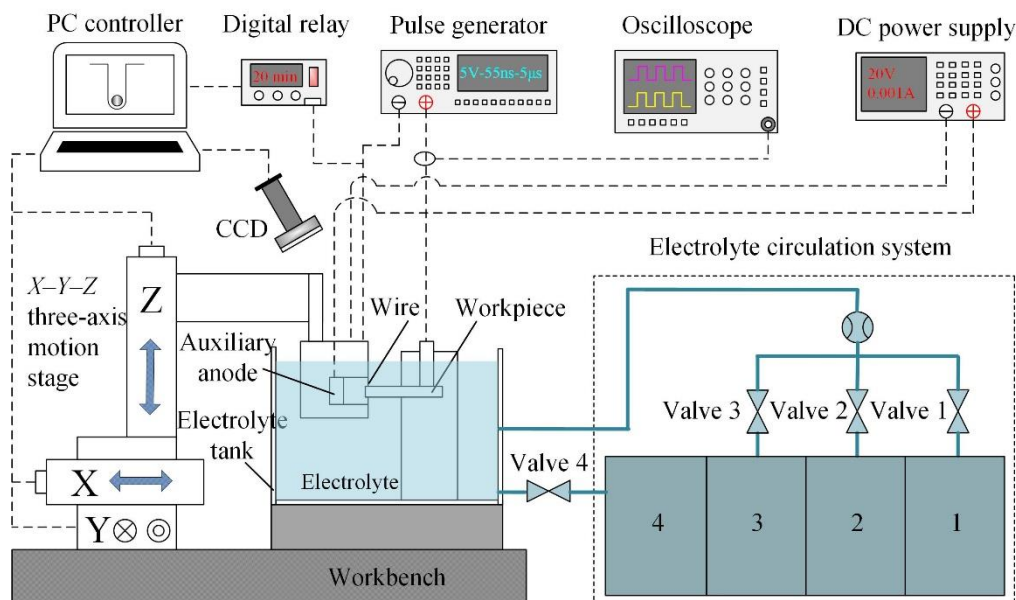


Figure 4. Schematic of the experimental system.

4. RESULTS AND DISCUSSION

4.1. WECMM before the electrochemical deposition

Based on the results of machining pre-trials and our previous work [19], the parameter values listed in Table 2 were selected for the WECMM.

Table 2. The selected parameters combination for WECMM of pure-nickel.

| Parameter | Value |
|--------------------------|------------------------|
| Wire vibration amplitude | 150 μm |
| Wire vibration frequency | 2 Hz |
| Applied voltage | 5 V |
| Feed rate | 0.25 $\mu\text{m/s}$ |
| Pulse width and period | 55 ns, 5 μs |
| Electrolyte | 0.1 mol/L HCl |

Fig. 5 shows the machining result by using the above machining parameters, and it can be seen that the width homogeneity of the machined micro-slit was relatively good, and there was no short circuit occurred during the machining process. Therefore, the same machining conditions were used to complete all the WECMM experiments before the electrochemical deposition in this study.

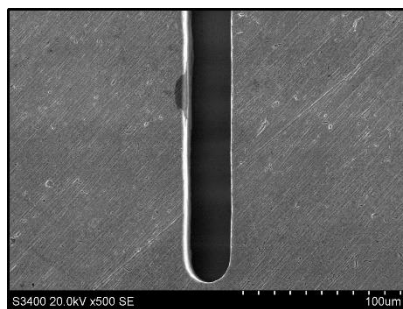


Figure 5. SEM example of the machined micro-slit.

4.2. Optimization of the electrochemical deposition

Fig. 6(a) shows the initial state before the electrochemical deposition. It can be seen that the wire was bright and its surface was clean. As the electrochemical deposition proceeded, the reduced metal ions were gradually deposited on the clean wire electrode surface until the machining gap was completely filled, as shown in Fig. 6(b).

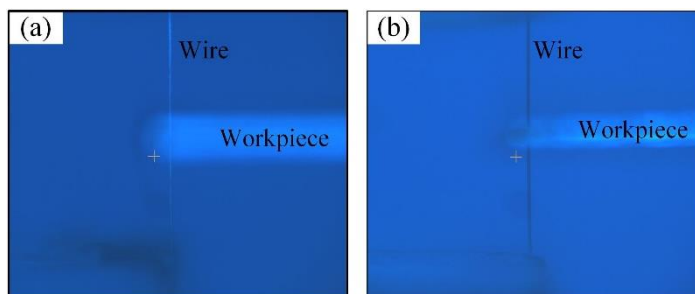


Figure 6. CCD examples of the enlarged wire and workpiece: (a) before the electrochemical deposition, (b) during the electrochemical deposition.

Selection of the right current density is very important for electrochemical deposition. Fig. 7 shows the electrochemical deposition results after 3 h under different current densities of 0.5 A/dm^2 , 1.0 A/dm^2 , and 2.0 A/dm^2 . When the current density was 0.5 A/dm^2 , it can be seen that the reduced metal ions have not been deposited on some areas on the wire surface, as shown in Fig. 7(a). Such areas with no deposition may also exist in the machining gap, which would mean that the machining gap has not been filled with the reduced metal ions. This would result in the failure of the experiment. However, when the current density was 2.0 A/dm^2 , there is inhomogeneous deposition on the surface of the wire and the grain size is rather large, as shown in Fig. 7(c). This may result in a deviation of the position of the wire in the machining gap. When the current density was 1.0 A/dm^2 , a uniform and dense electrochemical deposition layer was observed on the surface of the wire. The electrodeposition in the machining gap was better, as shown in Fig. 7(b). This result agrees with the report of Li *et al.* [20], which showed that the current density is too high or too small to achieve the desired results. Therefore, 1.0

A/dm^2 was selected as the appropriate current density in this paper.

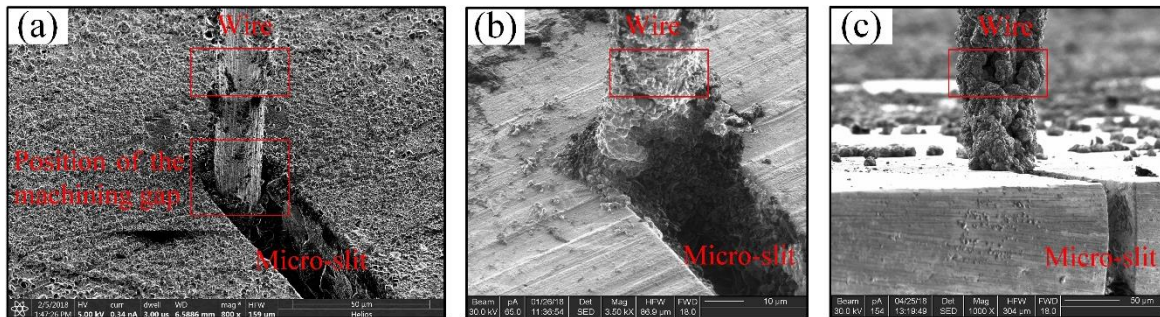


Figure 7. SEM examples of the electrochemical deposition results with different current densities: (a) $0.5 A/dm^2$, (b) $1.0 A/dm^2$, and (c) $2.0 A/dm^2$.

Fig. 8 shows a verification whether the wire was fixed by electrochemical deposition layer with a current density of $1.0 A/dm^2$. The wire fixture was moved in the opposite direction to that used in WECMM. It can be seen that wire has bent to a considerable degree due to the reverse movement, which indicates that the wire was firmly fixed in the machining gap by the electrochemical deposition layer.

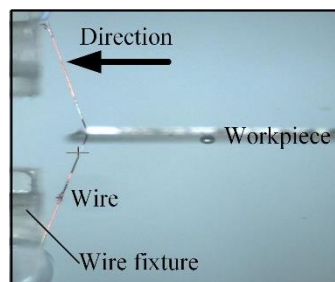


Figure 8. CCD example of the validation for showing the bend in the wire.

The duration of the electrochemical deposition is also very important for obtaining good results. Fig. 9 shows the electrochemical deposition after 6 h at a current density of $1.0 A/dm^2$. Reduced metal ions were deposited in large areas around the micro-slit. This occurred because when the gap became filled with reduced metal ions, the workpiece became part of the cathode, just like the wire. It would be more difficult to obtain a clear view of the contour of the machining gap if too many metal ions were deposited around the micro-slit. However, if the electrochemical deposition time were too short, then the machining gap might not become filled by the reduced metal ions. Repeated experiments showed that better result was obtained after 3 h of electrochemical deposition.

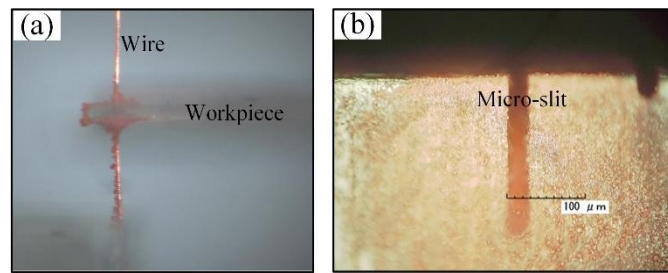


Figure 9. Examples of electrochemical deposition after 6 h: (a) CCD image of the enlarged wire and workpiece, and (b) digital microscope image of electrochemical deposition area.

After the electrochemical deposition was completed using the optimized parameters, the fixed wire was separated from the wire fixture, the wire and workpiece combination was obtained. Fig. 10 shows the results, it can be seen that the separated wire was well fixed in the position of the machining gap, the wire and workpiece combination with a clear micro-slit structure contour were obtained.

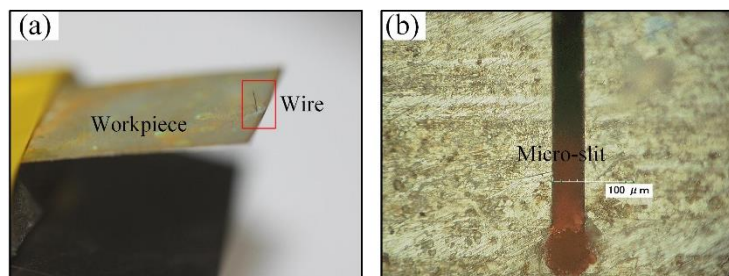


Figure 10. Examples of the electrochemical deposition results by using the optimized parameters: (a) digital camera image of the wire and workpiece combination, (b) digital microscope image of electrochemical deposition area.

4.3. Selection of the methods for obtaining clear machining gap contour

After the electrochemical dissolution, the machining gap area and wire surface were covered by the electrochemical deposition layer. In order to reveal a clear contour of the machining gap, redundant wire and deposited metals beyond the workpiece surface need to be removed. In this step, all the experiments were carried out after accomplishing the electrochemical deposition process.

Precision grinding was tried first. The wire and workpiece combination was first coated with cured epoxy resin. Then, it was ground along the surface parallel to the workpiece. However, the force produced by grinding causes the micro-slit to deform, which destroys the contour of the machining gap. Moreover, the grinding is uneven and cannot consistently remove material, so that the contour of the machining gap is not clearly visible, as shown in Fig. 11(a). In addition, the methods of picosecond laser cutting and electrical discharge machining (EDM) were also tried. However, the machining gap contour cannot be clearly presented, as shown in Fig. 11(b) and Fig. 11(c). This is because that these two methods are the thermal process, the recast layers caused by machining prevents the machining gap from being

clearly revealed, which can be explained more specifically according to the reports of Hendijanifard *et al.* [21] and Song *et al.* [22].

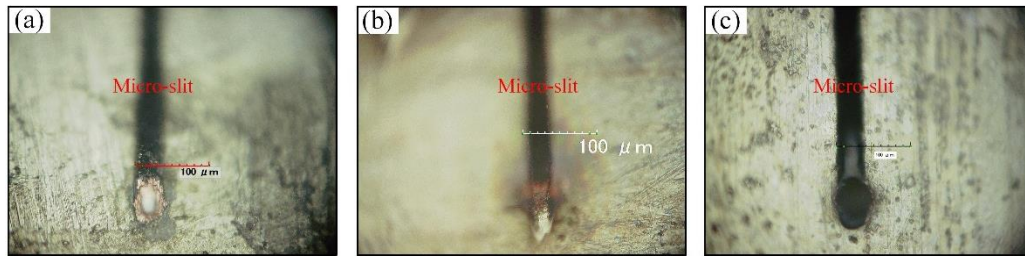


Figure 11. Digital microscope examples of the tried methods for removing the redundant wire and metal deposited beyond beyond the workpiece surface: (a) precision grinding, (b) picosecond laser cutting, and (c) electrical discharge machining.

Focused ion beam (FIB) technology has become increasingly attractive in the fabrication of nanoscale structures [23]. In the material removal, when the ion beam is irradiated on the solid surface, all surface atoms will receive energy. If this energy is bigger than the surface binding energy, the surface atoms will be sputtered [24]. In this paper, focused ion beam milling (sputtering and etching) was used to remove the redundant metals and wire beyond the workpiece surface. This method does not damage the original state of the machining gap. A focused ion beam system (Strata FIB 201, FEI Co., America) was used to perform focused ion beam milling.

Fig. 12 shows the machining gap after focused ion beam milling. It can be seen that the contour of the machining gap is clearly revealed in all the examples. In contrast to Fig. 5, the position of the wire relative to the micro-slit was maintained by the electrochemical deposition layer, the instantaneous machining gap produced by WECMM under the machining condition in Table 2 was obtained.

In WECMM, the workpiece material within the machining gap is removed in the form of ions using nanosecond pulses. However, at the end of WECMM, the simultaneous shutting down of the pulse generator and the halting of the feeding of the wire cannot be precisely controlled in each experiment at the nanosecond level, and the experimental errors are inevitable after a series of processes, so some subtle differences were observed after comparing Fig. 12(a), Fig. 12(b), and Fig. 12(c). From the instantaneous machining gap obtained by the proposed method, accurate values for the side gap, normal gap, and end gap specifically can be obtained. As a result, the formation and distribution of the instantaneous machining gap under the machining condition in Table 2 can be further studied. Thus, the method proposed in this paper provides experimental possibilities for revealing the regularities of WECMM.

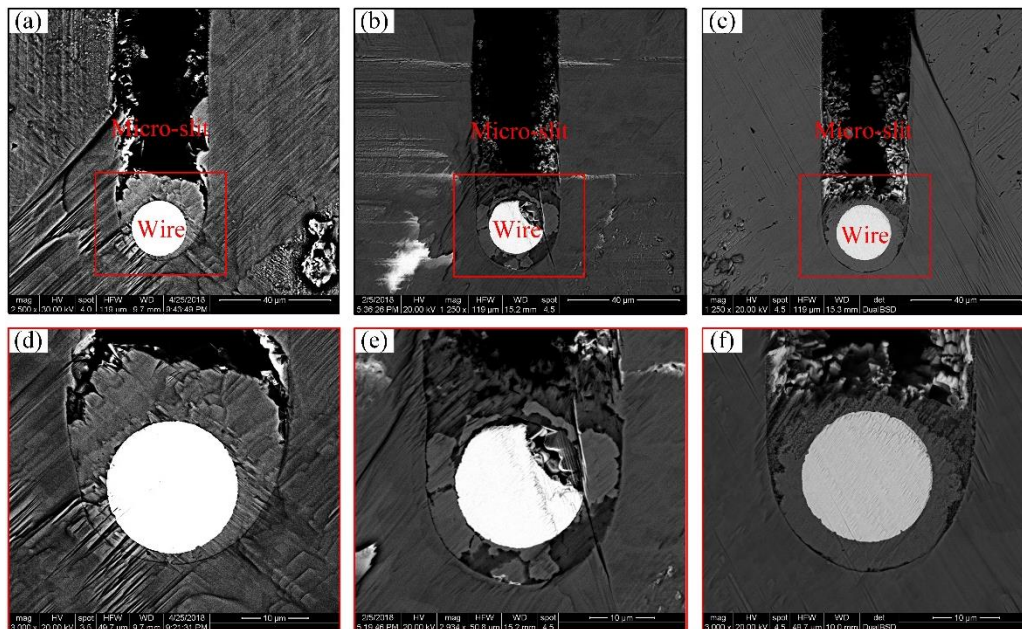


Figure 12. SEM examples of the integral topography of the obtained machining gap: (a) example 1, (b) example 2, and (c) example 3. SEM examples of the corresponding local topography for: (d) example 1, (e) example 2, and (f) example 3.

5. CONCLUSIONS

A method for revealing the instantaneous machining gap produced during WECMM has been proposed and investigated. The conclusions can be summarized as follows:

- (1) Simulation analysis show that reduced metal ions can be deposited onto the wire surface when the wire is in a micro-slit produced by WECMM.
- (2) The experimental results show that the position of the wire relative to the micro-slit in the narrow machining gap can be maintained by electrochemical deposition, the current density of 1.0 A/dm^2 and machining time of 3 h were obtained as the appropriate process parameters.
- (3) Compared with precision grinding, picosecond laser cutting, and electrical discharge machining, focused ion beam milling is better at removing unwanted material and clearly revealing the contour of the machining gap without damage to the original state of the gap.
- (4) The proposed method provides possibilities for further experimental studies of the formation and distribution of the machining gap.

ACKNOWLEDGMENT

This project was supported by the National Natural Science Foundation of China (51775276), the Natural Science Foundation of Jiangsu Province (BK20192007), and the Postgraduate Research & Practice Innovation Program of Jiangsu Province (KYCX19_0163).

References

1. C. Gao, N. Qu, B. Ding, Y. Shen, *Electrochim. Acta*, 295 (2019) 67–74.
2. L. Meng, Y. Zeng, D. Zhu, *J. Electrochem. Soc.*, 165 (2018) E665–E673.
3. F. Klocke, T. Herrig, M. Zeis, A. Klink, *Procedia CIRP*, 68 (2018) 725–730.
4. Y. Zhang, M. Kang, H. Li, Y. Liu, *Int. J. Electrochem. Sci.*, 14 (2019) 6032–6044.
5. S. Debnath, B. Doloi, B. Bhattacharyya, *J. Electrochem. Soc.*, 166 (2019) E293–E309.
6. S. Debnath, J. Kundu, B. Bhattacharyya, *J. Electrochem. Soc.*, 165 (2018) E35–E44.
7. W. Xiangyang, F. Xiaolong, Z. Yongbin, Q. Ningsong, *Int. J. Electrochem. Sci.*, 11 (2016) 7216–7229.
8. T. Yang, Y. Zeng, X. Fang, Y. Li, *Int. J. Electrochem. Sci.*, 15 (2020) 1691–1703.
9. K. Xu, Y. Zeng, P. Li, X. Fang, D. Zhu, *J. Mater. Process. Technol.*, 235 (2016) 68–74.
10. H. He, N. Qu, Y. Zeng, X. Fang, Y. Yao, *Int. J. Adv. Manuf. Technol.* (2016) 2353–2359.
11. L. Meng, Y. Zeng, X. Fang, D. Zhu, *Intermetallics*, 81 (2017) 16–25.
12. N. Qu, X. Fang, W. Li, Y. Zeng, D. Zhu, *Chinese J. Aeronaut.*, 26 (2013) 224–229.
13. F. Xiaolong, Z. Xianghe, Z. Pengfei, Z. Yongbin, Q. Ningsong, *Int. J. Adv. Manuf. Technol.*, 84 (2016) 929–939.
14. Z. Xianghe, F. Xiaolong, Z. Yongbin, Z. Pengfei, Z. Di, *Int. J. Electrochem. Sci.*, 11 (2016) 2335–2344.
15. L. Meng, Y. Zeng, X. Fang, D. Zhu, *J. Alloys Compd.*, 739 (2018) 235–248.
16. H.D. He, N.S. Qu, Y.B. Zeng, Y.Y. Yao, (2017) 3177–3186.
17. D. Zhu, K. Wang, N.S. Qu, *Ann. Cirp*, 56 (2007) 241–244.
18. V.M. Volgin, V. V. Lyubimov, V.D. Kukhar, A.D. Davydov, *Procedia CIRP*, 37 (2015) 176–181.
19. X. Bi, Y. Zeng, N. Qu, *Precis. Eng.*, 61 (2020) 14–22.
20. A. Li, X. Tang, Z. Zhu, Y. Liu, *Int. J. Adv. Manuf. Technol.*, 101 (2019) 3055–3064.
21. M. Hendijanifard, D.A. Willis, *Phot. Process. Microelectron. Photonics VII*, 6879 (2008) 687907.
22. S. Mancang, D. Liqun, L. Chong, L. Junshan, L. Ying, *Key Eng. Mater.*, 609–610 (2014) 1521–1525.
23. A.A. Tseng, *Small*, 1 (2005) 924–939.
24. C.S. Kim, S.H. Ahn, D.Y. Jang, *Vacuum*, 86 (2012) 1014–1035.

© 2020 The Authors. Published by ESG (www.electrochemsci.org). This article is an open access article distributed under the terms and conditions of the Creative Commons Attribution license (<http://creativecommons.org/licenses/by/4.0/>).